Spectral and magnetic properties of one-dimensional superlattices

1998 J. Phys.: Condens. Matter 10 4755

(http://iopscience.iop.org/0953-8984/10/22/005)

J. Phys.: Condens. Matter **10** (1998) 4755–4776. Printed in the UK PII: S0953-8984(98)89201-1

Spectral and magnetic properties of one-dimensional superlattices

Dariusz Góra, Krzysztof J Rościszewski and Andrzej M Oleś
Institute of Physics, Jagellonian University, Reymonta 4, PL-30059 Kraków, Poland

Received 13 November 1997

Abstract. We investigated the electron correlation effects in one-dimensional superlattices composed of free (uncorrelated) and repulsive (correlated) sites, using Lanczos diagonalization of chains of up to ten sites described by a Hubbard-like Hamiltonian. The electronic and magnetic properties are shown to depend primarily on the splitting between single-site energies for the correlated and uncorrelated orbitals, respectively, and on the average electron density in the system. The local moments and spin–spin correlations are closely related to the changes in the conductivity, and the magnetic properties are enhanced when the insulating regime is approached. Irrespective of the type of superlattice considered, the local moments form on the correlated orbitals, and may only be induced on single uncorrelated orbitals which separate correlated clusters. The transition from metallic to insulating behaviour can be qualitatively understood in terms of a strongly correlated model, with two Hubbard subbands due to strong Coulomb interactions accompanied by a metallic band of uncorrelated states.

1. Introduction

Materials of the superlattice type are of great interest both as regards theory and applications as they exhibit a rich variety of novel physical properties. For example, three-dimensional samples built up of alternating metallic magnetic (Fe, Ni or Co atoms) and metallic nonmagnetic (Cu, Ag, Mn, Au or Mg atoms) layers show gigantic magnetoresistance or spectacular oscillations of local magnetic moments due to modifications of the thickness of the individual layers [1–4]. Thus, it is clear that nonrandom inhomogeneous systems of strongly correlated electrons are very different from the relatively well studied and understood homogeneous systems. Developing an at least qualitative electronic theory of the magnetic properties of superlattices (starting from first principles) is a hard task. It is therefore much more promising to start from a simple model which still contains the essential physics, and allows one to understand the mechanism responsible for the changes of the magnetization. Following this idea, Paiva and Santos [5] studied a one-dimensional (1D) Hubbard-type model of a superlattice with a single s orbital per site. Metallic superlattice layers were mimicked by alternating free sites, with Coulomb on-site interaction $U = 0$, and insulating nonmagnetic layer sites, with significant Coulomb repulsion $U > 0$. The superlattice atoms are coupled by the usual kinetic part (a hopping term). To simplify the analysis, Paiva and Santos assumed that the on-site orbital energy was exactly the same for all of the sites (i.e., both in metallic and in insulating layers).

In spite of the fact that the model was a drastic oversimplification, it revealed novel and interesting physical mechanisms which could be relevant to a future more realistic

0953-8984/98/224755+22$19.50

theory of magnetic–nonmagnetic three-dimensional superlattices. On one hand, at half-filling a weak form of frustration that was nevertheless sufficient to wipe out the strong spin-density correlations (characteristic of homogeneous systems) was demonstrated. On the other hand, spin-density correlations appeared for some superlattices away from half-filling. Below half-filling the local magnetic moments were sometimes displaced from repulsive to free (metallic) sites. There were also some other observations, as many simple types of correlation function which characterize the system were calculated [5]. Although the results of reference [5] were novel and appealing as regards providing an intuitive feel for the physics, they require further study for a more general situation. This task is undertaken in the present paper.

First, we released the artificial assumption of the absence of splitting between single-site energies for correlated and uncorrelated orbitals. Second, we decided to study not only the ground-state properties and ground-state correlation functions, but also the spectral functions and optical conductivity, including the behaviour of the Drude peak under doping. The reason for this is that local magnetic moments and spin–spin correlations are closely related to changes in the conductivity [6]. Moreover, spin–spin correlation enhancement can be expected when the insulating regime is approached.

We aim to achieve a better understanding of how the splitting of orbital energies (i.e., finite charge-transfer energy), the average electron filling, and the specific superlattice structure influence the electronic and magnetic properties of the systems studied. However, with so many parameters and other factors influencing the electronic and magnetic properties, some simple model capable of providing a qualitative description of the systems is highly desirable. In the following we will propose such a model.

The paper is organized as follows. In section 2 the model Hamiltonian is introduced, and the details of the exact-diagonalization method are discussed. In section 3 we summarize the basic facts concerning the optical conductivity and the Drude peak for homogeneous systems, and contrast them with those for a superlattice. In section 4 we introduce the above-mentioned model, and confirm its validity through the computation of spectral density functions for photoemission and inverse photoemission. Section 5 contains the data concerning local magnetic properties and intersite spin–spin correlations for half-filling and away from it. The paper is closed with a short summary and a discussion of general implications of the results presented in section 6.

2. The model

We consider 1D superlattices which consist of periodic arrangements of two kinds of atom, without and with on-site Coulomb interaction U, described by the Hamiltonian

$$H = \varepsilon_0 \sum_{i\in F,\sigma} c^\dagger_{i\sigma} c_{i\sigma} + \varepsilon_U \sum_{i\in R,\sigma} c^\dagger_{i\sigma} c_{i\sigma} + \sum_{i\sigma} t_{i,i+1}(c^\dagger_{i,\sigma} c_{i+1,\sigma} + \mathrm{HC}) + U \sum_{i\in R} n_{i\uparrow} n_{i\downarrow} \qquad (1)$$

where $c^\dagger_{i,\sigma}$ ($c_{i,\sigma}$) are creation (annihilation) operators for an electron with spin σ at site i, and $n_{i\sigma} = c^\dagger_{i\sigma} c_{i\sigma}$ are electron number operators. The first two terms of the Hamiltonian stand for the orbital energy, ε_i, which takes one of two values: ε_0 or ε_U, depending on whether the orbital belongs to a free atom ($i \in F$), or to an atom with Coulomb interaction U ($i \in R$). The positions of free atoms are specified by the set F, while the positions of repulsive atoms, with $U > 0$, are specified by the set R. These sets exhaust the entire lattice, and one recovers the usual Hubbard Hamiltonian [7] if all of the atoms belong to the set R.

The third term describes the kinetic energy T, while the fourth term is the on-site Coulomb repulsion U. This corresponds to the real structure of the superlattice in three dimensions, consisting of an alternating sequence of 'free layers' ($U_i = 0$ for all sites within the layer) and 'repulsive layers' ($U_i > 0$). We follow here (as far as possible) the terminology introduced by Paiva and Santos [5]. In our case we focus on the direction normal to the layers, and consider different textures characterized by the number of free sites denoted as L_0, accompanied by the corresponding number of repulsive sites L_U. The pattern of L_0 free sites and L_U repulsive sites alternates, and we simulate such systems by diagonalizing finite clusters of N sites.

The specific values of the model parameters as well as the appropriate boundary condition (when working with the finite clusters) are of great importance. For 1D systems at half-filling ($n = 1$), the so-called modified periodic boundary conditions (MBC) are one possibility [8]. For MBC, when $M = 4m$, where m is a natural number, true periodic boundary conditions (PBC) are used, whereas for $M = 4m+2$ one uses instead antiperiodic boundary conditions (ABC). This choice follows from the different behaviours of linear clusters with $M = 4m$ and $M = 4m + 2$ sites, respectively [8–10]. In practice PBC and ABC are implemented in a cluster with torus topology (a circle); the terminal hopping integral $t_{N,N+1} \equiv t_{N,1}$ in the case of PBC is taken as the normal hopping constant, but for ABC it is taken with the opposite sign instead [9]. For the optical conductivity, we consider also the so-called free boundary conditions (FBC) for which the clusters stay linear, and $t_{N,N+1} \equiv t_{N,1} \equiv 0$. In general, however, FBC usually give much less good results for really small clusters than the MBC because boundary effects (versus bulk effects) are more pronounced for the FBC.

In the following we employed a more reliable and simple approach: in each case, i.e., for any lattice and any filling n, we calculate the ground-state energy for both PBC and ABC, and choose the boundary conditions which give a lower energy.

It is well known that the Lanczos method [12–14] is an excellent tool for obtaining exact results for the ground states of finite clusters [15, 16, 11, 17], and we employ it in the present work. In order to achieve a good physical insight and investigate in more detail the dependence on the parameters, we consider relatively small clusters. Here we apply Lanczos diagonalization to the models of superlattices, and investigate the properties of the system by varying the energy splitting between the on-site energies (charge-transfer energy), $\Delta = \varepsilon_0 - \varepsilon_U$, Coulomb interaction U, and electron filling n. For convenience, ε_U is chosen as a global reference zero energy for all of the systems studied, and ε_0 is the parameter to be varied. We use $t_{i,i+1} = -1$ eV as the energy unit. Thereby, we do not distinguish between t_{0-0}, t_{0-U}, and t_{U-U}, which denote the hopping constants for hopping between nearest-neighbour sites, between either two sites both belonging to free layers, or two different sites, one belonging to free and the second to a repulsive layer, or, finally, between two sites both belonging to repulsive layers, respectively (the subscripts are self-explanatory). Several calculations were performed for fixed $U = 4|t|$ which corresponds to intermediate correlations, as encountered in real transition metals. We also varied U to investigate the changes in the magnetic correlations from weakly to strongly correlated systems. The electron filling is given by the ratio $n = (N_\uparrow + N_\downarrow)/M$, where $N_\uparrow$ and $N_\downarrow$ are the total numbers of up and down electrons in the cluster of M sites, respectively. In the following, if not stated otherwise, nonmagnetic clusters with $N_\uparrow = N_\downarrow$ are analysed.

Using the standard Lanczos packet we obtained data for:

(i) the ground-state energy E_0,
(ii) the kinetic energy K,

(iii) the average on-site occupation numbers $\langle n_{i\sigma}\rangle$,
(iv) the average double occupations $\langle n_{i\sigma}n_{i,-\sigma}\rangle$ per site,
(v) the charge–charge correlation functions $\langle n_{i\sigma}n_{i+1,\sigma}\rangle$ (nearest neighbours) and $\langle n_{i,\sigma}n_{i+2,\sigma}\rangle$ (next-nearest neighbours),
(vii) the local moments $\langle \boldsymbol{S}_i^2\rangle$, and
(viii) the spin–spin correlations functions $\langle \boldsymbol{S}_i \cdot \boldsymbol{S}_j\rangle$.

Moreover, we determined the optical conductivity, which gives information about whether the behaviour is insulating or metallic, and the spectral functions. These results are reported in sections 3, 4, and 5.

3. Optical conductivity

3.1. The Drude peak for homogeneous system

We start the discussion with the optical conductivity $\sigma(\omega)$ at zero temperature, defined in a standard way [19–22],

$$\sigma(\omega) = D\delta(\omega) + \sigma_{reg}(\omega). \tag{2}$$

The first term in equation (2) corresponds to direct-current conduction due to the constant external electric field. The precise value of the conductivity is defined by the magnitude D of the Drude peak; if $D = 0$ one finds an insulator. The value of D can be obtained from the following formula [23]:

$$D = -\frac{\pi}{N}\langle\psi_0^N|T|\psi_0^N\rangle + \pi \,\mathrm{Re}\,\chi(\omega \to 0) \tag{3}$$

where $\chi(\omega)$ is given by [23]

$$\sigma_{reg}(\omega) = -\frac{1}{\omega N}\,\mathrm{Im}\,\chi(\omega) \tag{4}$$

where the current operator j_p (defined for the wave vector $\boldsymbol{q} = 0$) is [24]

$$j_p = \mathrm{i}\sum_{i,\sigma} t_{i,i+1}(c_{i+1,\sigma}^{\dagger}c_{i,\sigma} - c_{i,\sigma}^{\dagger}c_{i+1,\sigma}). \tag{5}$$

In a different (but equivalent) form, D can be given as

$$D = -\frac{\pi}{N}\langle\psi_0^N|T|\psi_0^N\rangle - \frac{2\pi}{N}\sum_{n\neq 0}\frac{|\langle\psi_n^N|j_p|\psi_0^N\rangle|^2}{\varepsilon_n - \varepsilon_0} \tag{6}$$

or, using more compact notation,

$$D = -\frac{\pi}{N}\langle\psi_0^N|T|\psi_0^N\rangle - 2\int_0^{\infty}\mathrm{d}\omega\ \sigma_{reg}(\omega). \tag{7}$$

These two forms of D, equations (6) and (7), will turn out to be useful in the arguments to follow. The second term in equation (2), i.e., $\sigma_{reg}(\omega)$, is related to optical transitions to the excited states (therefore it is frequently called the optical absorption), and can be expressed using the following formula [23–25]:

$$\sigma_{reg}(\omega) = \frac{\pi}{\omega N}\sum_{n\neq 0}|\langle\psi_0^N|j_p|\psi_n^N\rangle|^2\delta[\omega - (\varepsilon_n - \varepsilon_0)] \tag{8}$$

or equivalently as

$$\sigma_{reg}(\omega) = -\frac{1}{\omega N}\,\mathrm{Im}\,\langle\psi_0^N|j_p^{+}\frac{1}{\omega + \varepsilon_0 - H + \mathrm{i}\eta}j_p|\psi_0^N\rangle \tag{9}$$

where $|\psi_n^N\rangle$ denotes the nth excited eigenstate of the system filled by N electrons, corresponding to the eigenenergy ε_n, and $|\psi_0^N\rangle$ stands for the ground-state eigenvector. (Here we use units where $c = e = \hbar = 1$, as in reference [23].) The evaluation of the optical conductivity using equation (9) is done in practice using the Lanczos method combined with continued-fraction expansion [15, 16].

As already emphasized, the value of D serves as an indication of whether the system under consideration is an insulator or a conductor. In the latter case, $D \neq 0$, while in the former one, $D = 0$. Therefore for the 1D (homogeneous) Hubbard model, D can be chosen as the order parameter for the conductor-to-insulator phase transition [23, 24]. While this criterion applies to an infinite 1D system, the only practical way to proceed for finite clusters is to extrapolate the D-value which corresponds to an infinite system from the set of D_M obtained for several clusters of different sizes using finite-size scaling. This task is difficult in the present case, as the sign of D_M oscillates when one varies the boundary conditions and/or such parameters as the cluster size M and the electron filling n. In particular, for the half-filled ($n = 1$) Hubbard model with $U > 0$ one finds that D_M tends to zero like an exponential function for $M = 4m$ clusters. However, for ABC, $D_{4m} > 0$, while for PBC, $D_{4m} < 0$ [23, 24]. A similar behaviour is found also for $M = 4m + 2$ clusters; however, each of the D_M forms two branches with opposite signs for D: for ABC, $D_{4m+2} < 0$, whereas for PBC, $D_{4m+2} > 0$.

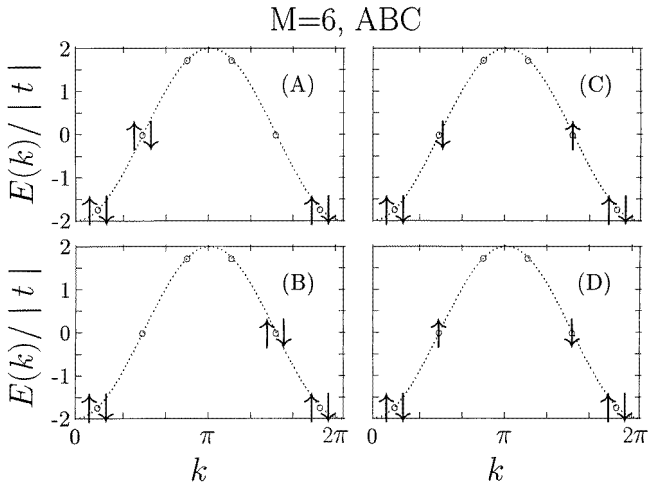

Figure 1. Energy levels in the Hartree–Fock approximation for the half-filled homogeneous system with $M = 6$ sites. For $U = 0$, the ground-state energies for the configurations shown in panels (A)–(D) are degenerate. On switching on finite U, the degeneracy is lifted, but different configurations are mixed within the matrix elements of the current operator.

The phenomenon of the sign of D_M changing according to the chosen boundary conditions can be qualitatively understood as follows. First of all, depending on the type of boundary conditions used, one has either a closed-shell or an open-shell system for a given cluster with an even number of sites (to avoid pathological situations, we do not consider odd-site clusters here). For example, the cluster of $M = 6$ sites filled by six electrons ($n = 1$) is a closed-shell system with PBC, but becomes an open-shell system if the ABC are used. Four configurations, (A)–(D), degenerate at $U = 0$ are shown in figure 1. When finite U is switched on, the degeneracy disappears, but these configurations are strongly

mixed within the matrix elements of the current operator (compare, e.g., reference [23]). In fact, the resulting matrix elements in equation (6) can be in this case so large that the second term on the right-hand side of equation (6) overwhelms the first (kinetic) term, and the amplitude of the Drude peak is negative ($D < 0$). In contrast, in a closed-shell system the ground state at $U = 0$ in nondegenerate, so no mixing between different configurations occurs in the current operator, and the second term is not large. Thus, the kinetic term dominates and the resulting Drude peak is positive $D > 0$. Taken together, these features explain why by changing the boundary conditions or by considering systems of increasing size with fixed boundary conditions, one may obtain a similar situation, i.e., oscillation of the sign of D. We note that for the systems below half-filling ($n < 1$), D is approximately proportional to $\pm|n - 1|$, and the sign oscillation phenomenon was not reported [23, 24].

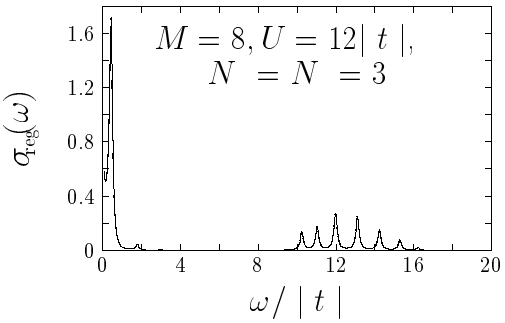

Figure 2. The regular part of the optical conductivity $\sigma_{reg}(\omega)$ as a function of $\omega/|t|$ for the Hubbard model with $M = 8$ sites ($L_0 = 0$, $L_U = 8$) with FBC, filled by $N_\uparrow = N_\downarrow = 3$ electrons, as obtained for $\varepsilon_0 = 0$ and $U = 12|t|$.

Now let us consider the case of FBC. The Drude peak for an open system has to vanish, as no direct current is possible if the system is open. In contrast, one knows that for the infinite system the Drude peak must be the same regardless of which boundary conditions have been used. Although there seems to be a contradiction, in fact the so-called Drude precursor (DP) appears for metallic clusters of finite size, with the spectral weight centred not at $\omega = 0$, but at a small finite energy ω (see figure 2). When the number of sites N grows to infinity, the DP gradually shifts towards zero. The appearance of the DP directly influences the susceptibility $\chi(\omega)$, and as a result equation (3) is not valid when FBC are used. Still, the value of D can be obtained even for FBC simply by measuring the area of the precursor peak. Alternatively, one can extract the DP weight from the spectra, compute the area under the remaining spectral curve, and use equation (7) to determine D. One must realize, however, that these methods can be inaccurate, and the extraction of the DP from the remaining spectra can be problematic (for example, in systems with small U when low-energy excitations do mix with the precursor). Nevertheless, if the DP is absent altogether, this shows that the system is an insulator.

We close this section with the total sum rule:

$$\int_0^\infty \mathrm{d}\omega\ \sigma(\omega) = -\frac{\pi}{N}\langle\psi_0^N|T|\psi_0^N\rangle. \tag{10}$$

This allows for an internal check in the course of the computations of the conductivity. In the large-U limit, the optical conductivity consists of two Hubbard subbands (figure 2) which obey separate sum rules, and are determined by local correlation functions [6].

3.2. The Drude peak for a superlattice

It is interesting to consider how the optical conductivity changes for a superlattice, and under which conditions a given superlattice is metallic. We found that some of the properties of the Drude peak reported for homogeneous systems are not valid for superlattices. We consider first the $M = 8$ cluster with $L_0 = 2$ and $L_U = 2$ for $\varepsilon_0 = \varepsilon_U = 0$, and vary the electron filling n. The selected numerical results for the Drude peak intensities computed using equation (3) are displayed in table 1.

Table 1. The Drude peak weight D_8 and selected correlation functions for the cluster of $M = 8$ sites, with $L_0 = L_U = 2$ and $\varepsilon_0 = 0$.

n	BC	D_8	$\overline{\langle n_{0\sigma}\rangle}$	$\overline{\langle n_{U\sigma}\rangle}$	$\overline{\langle S_0^2\rangle}$	$\overline{\langle S_U^2\rangle}$
1.75	PBC	0.064	0.989	0.760	0.015	0.359
1.50	ABC	−0.095	0.969	0.530	0.045	0.601
1.25	PBC	2.524	0.794	0.455	0.260	0.536
1.00	ABC	3.184	0.628	0.371	0.377	0.465
0.75	PBC	3.299	0.460	0.289	0.381	0.386
0.50	ABC	2.364	0.318	0.181	0.334	0.257
0.25	PBC	1.495	0.134	0.115	0.178	0.169

First of all, we notice that unlike in a homogeneous system the sign of D oscillates when the boundary conditions are fixed, and the filling n increases and approaches half-filling. One finds $D > 0$ for $n = 0.25$, 0.75, 1.25, and 1.75, i.e., for unequal numbers of up- and down-spin electrons, and $D < 0$ for $n = 0.5$, 1.0, and 1.5, i.e., for equal numbers of up- and down-spin electrons. This happens if one takes the same PBC for all different n. However, if we fix the boundary conditions using the minimum-of-energy principle, the sign oscillation phenomenon can be avoided. In fact, our arguments given in section 3.1 (for the qualitative explanation of the sign oscillation phenomenon) apply also to the present case of a superlattice, but as the system consists of atoms of two kinds, one has to consider two separate dispersion curves, similar to those shown in figure 1: one for the free sites, and the second for the repulsive sites. If the ground state for a given filling is degenerate (for $U = 0$) when using PBC, one has to change to ABC instead. An example is the system with $L_0 = L_U = 2$ filled by $N = 2$ electrons (see table 1). Although this criterion is certainly an oversimplification, we have verified that it applies to the small clusters considered in the present study.

Our second observation is that the conductivity is gradually suppressed by the increasing Coulomb interaction U in the range of filling $n > 1.5$. At the value of $U = 4|t|$ considered, the one-particle levels for adding a second electron are, in the case considered, $\varepsilon_0 = 0$ and $\varepsilon_U + U = 4|t|$, and the holes localize. A similar situation is found for low electron filling, if $\varepsilon_0 = 4|t|$. This holds true for both PBC and ABC, and we conclude that the superlattice structure gives in general quite different conductivities in electronic and hole regimes, and the metallic behaviour is suppressed for $n \gg 1$ ($n \ll 1$) if the one-particle hole (electron) levels of free and correlated atoms are different from each other.

By analysing the numerical results for $\sigma_{reg}(\omega)$ we confirm all of the qualitative results discussed above. For $N_\uparrow = N_\downarrow = 1$, 3, and 5, one finds a metal (figure 3), with the pronounced Drude precursor peak formed when FBC are used (note, however, that the extraction of the Drude precursor peak from the data is not trivial). In contrast, the system filled by $N_\uparrow = N_\downarrow = 7$ electrons is an insulator, and no Drude precursor is found in figure 3(G).

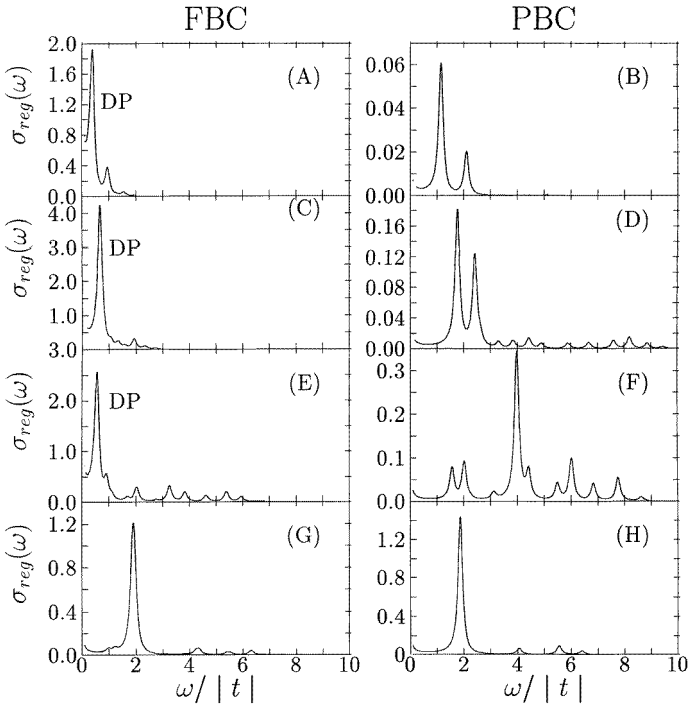

Figure 3. The regular part of the optical conductivity $\sigma_{reg}(\omega)$, as obtained using FBC (left) and PBC (right) for the cluster of $M = 8$ sites, $L_0 = L_U = 2$, $\varepsilon_0 = 0$, and $U = 4|t|$. Different panels correspond to different electron fillings: (A) and (B), $N_\uparrow = N_\downarrow = 1$; (C) and (D), $N_\uparrow = N_\downarrow = 3$; (E) and (F), $N_\uparrow = N_\downarrow = 5$; (G) and (H), $N_\uparrow = N_\downarrow = 7$. The Drude precursor (DP) is missing in case (G), and the system is then an insulator.

It might be expected that the area of the Drude peak would increase with the total electron number N in the cluster. In fact, the behaviour of the Drude peak is governed not just by the total electron count in the cluster, but also by the *individual filling of the free and repulsive sites* in the superlattice (in real space). These fillings can be controlled by varying the orbital energy ε_0 (while keeping N fixed). As an example, we give the numerical results in table 2 for three selected values of ε_0. Using our criterion of minimizing the total energy of the system, the closed-shell systems are more relevant, obtained by taking: PBC for $M = 6$, ABC for $M = 8$, and PBC for $N = 10$. The extrapolation to an infinite cluster gives in this case an insulating behaviour, represented by $D_\infty = 0$ for $\varepsilon_0 = -5|t|$. In contrast, for larger values of $\varepsilon_0 = 0$ and $2|t|$ one finds $D_\infty > 0$, and the systems are metallic. Thus, we conclude that the one-particle energies of the two kinds of atom in the superlattice have to be close to each other in order for one to obtain a metallic behaviour, and the most favourable case for metallic behaviour is given by $\varepsilon_0 = U/2$.

An example of numerical data for an $M = 6$ cluster with two subgroups of uncorrelated and free orbitals, $L_0 = L_U = 3$, is shown in figure 4. As for $L_0 = L_U = 1$ (table 2), using the FBC one finds an insulating behaviour for $\varepsilon_0 = -5|t|$ (figure 4(A)). The system changes gradually into a weak metal with increasing ε_0, and the DP occurs at the energy $\omega \simeq |t|$ (figures 4(C) and 4(E)). We note, however, that the metallic behaviour is much weaker than that for the alternating free and correlated orbitals in the $L_0 = L_U = 1$ case. This shows that the geometry of the superlattice plays an important role in the conductivity, and

Table 2. Selected Drude peak weights D_M for half-filled systems and for $L_0 = L_U = 1$. The boundary conditions used correspond to closed-shell systems with lower energy, and are indicated in round brackets. The Drude weight for the infinite system, D_∞, was obtained using exponential extrapolation, $\ln|D_M| = a + b/M$.

$\varepsilon_0/\|t\|$	D_6	D_8	D_{10}	D_∞
−5.0	0.066 (PBC)	0.009 (ABC)	0.002 (PBC)	0.00
0.0	2.697 (PBC)	2.092 (ABC)	1.585 (PBC)	0.75
2.0	3.721 (PBC)	3.576 (ABC)	3.494 (PBC)	3.18

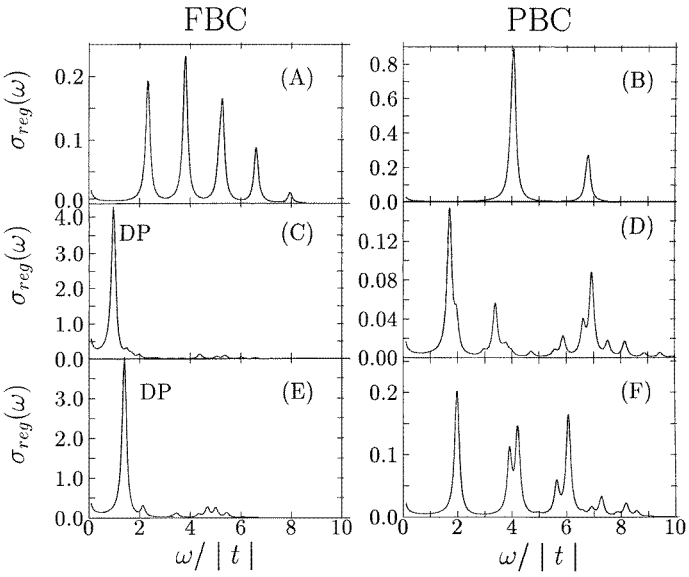

Figure 4. The regular part of the optical conductivity $\sigma_{reg}(\omega)$, as obtained using PBC (left) and FBC (right) for the cluster of $M = 6$ sites at half-filling, with $L_0 = L_U = 3$, $U = 4|t|$ at half-filling, for different values of ε_0: $-5|t|$ in (A) and (B), 0 in (C) and (D), and $2|t|$ in (E) and (F). Note that the precursor is mixed with low-energy excitations—using FBC to calculate D, the error can be estimated to be as large as 30–50%. Therefore one must use PBC for clusters with different sizes and subsequently extrapolate (compare tables 2 and 3).

the clusters of correlated orbitals rapidly suppress the metallic behaviour. In the clusters with PBC one finds a systematic change of $\sigma_{reg}(\omega)$, with the weight shifted to lower ω for increasing ε_0, and an increasingly weak Drude peak found for $\varepsilon_0 = 0$ and $\varepsilon_0 = 2|t|$ (figures 4(D) and 4(F)).

The results of a more systematic study of the gradual transition from an insulating to a metallic superlattice are summarized in table 3. Regardless of the average filling and the superlattice structure, the systems are insulating as long as $\varepsilon_0 \simeq -5|t|$, with a very low value of the extrapolated Drude weight, D_∞. The metallic behaviour is found when the degeneracy of the single-site levels ε_0 and ε_U is approached, and all of the systems studied with $n \leqslant 1$ are metallic for $\varepsilon_0 = -|t|$. For the systems below half-filling, one finds the best metals when the free levels are somewhat above the correlated levels, e.g., $\varepsilon_0 - \varepsilon_U \simeq |t|$. This is easily understandable, as the electron correlations partly suppress the metallic behaviour. In contrast, at half-filling the largest value of D_∞ in the $L_0 = 3$,

$L_U = 1$ clusters was found at $\varepsilon_0 - \varepsilon_U \simeq 2|t|$, i.e., for the particle–hole-symmetric spectrum.

The systems above half-filling are good metals for $\varepsilon_0 - \varepsilon_U \simeq U$, which follows from the particle–hole symmetry. As an example, we show the relevant results for the $L_0 = 1$, $L_U = 4$ cluster in table 3 for two fillings symmetric with respect to $n = 1$: $n = 0.8$ and $n = 1.2$. The extrapolated values of $D_\infty = 1.26$ found independently for $\varepsilon_0 = 5|t|$ at $n = 1.2$ and for $\varepsilon_0 = -|t|$ at $n = 0.8$ confirm the particle–hole symmetry of these clusters.

Table 3. Selected Drude peaks D_M for various clusters and fillings at $U = 4|t|$. D_{M1} was obtained for small clusters with a single unit cell, i.e., $M = L_0 + L_U$, using the boundary conditions indicated in round brackets. In every case the results correspond to minimal energy of the ground state (the closed-shell configuration). D_{M2} was obtained for larger clusters consisting of two unit cells, i.e., $M = 2(L_0 + L_U)$, with ABC (the closed-shell configuration). The Drude weight for the infinite system, D_∞, was obtained using exponential extrapolation, $\ln|D_M| = a + b/M$. A crude (pessimistic) estimate of the error which follows from the differences between the linear and exponential extrapolations is up to 0.5 for $L_0 = L_U = 1$, $n = 1$, for the clusters with $M = 6$, 8, and 10 sites.

L_0	L_U	n	$\varepsilon_0/\|t\|$	D_{M1}	D_{M2}	D_∞
2	2	0.5	−5.0	0.625 (PBC)	0.331	0.00
			−1.0	2.387 (PBC)	1.118	0.52
			0.0	2.934 (PBC)	2.364	1.90
			0.8	3.016 (PBC)	2.722	2.46
			2.0	2.405 (PBC)	1.174	0.57
			5.0	0.737 (PBC)	0.036	0.00
1	4	0.8	−5.0	1.570 (ABC)	0.390	0.10
			−1.0	2.973 (ABC)	1.933	1.26
			0.0	3.352 (ABC)	2.694	2.16
			0.8	3.486 (ABC)	3.080	2.72
			2.0	3.084 (ABC)	2.019	1.32
			5.0	1.438 (ABC)	0.161	0.02
3	1	1.0	−5.0	2.130 (ABC)	0.520	0.13
			−1.0	3.744 (ABC)	2.490	1.66
			0.0	4.056 (ABC)	3.263	2.63
			0.8	4.191 (ABC)	3.649	3.18
			2.0	4.250 (ABC)	3.828	3.47
			5.0	3.744 (ABC)	2.490	1.66
1	4	1.2	−5.0	0.734 (PBC)	0.033	0.00
			−1.0	1.438 (PBC)	0.160	0.02
			0.0	1.831 (PBC)	0.314	0.05
			0.8	2.273 (PBC)	0.629	0.17
			2.0	3.084 (PBC)	2.038	1.35
			5.0	2.973 (PBC)	1.932	1.26

4. One-particle excitations

4.1. A toy model of two noninteracting sublattices

Before we discuss the densities of states as obtained for the clusters which model a superlattice, let us introduce a simplified model (called below the toy model) in which the superlattice can be treated as two disjoint subsystems: the first one consists of free sites,

while the second is composed of repulsive sites. This might be realized by assuming the atomic limit, $t_{ij} = 0$, but also could be realized by considering a long-distance hopping limited to atoms of the same kind, i.e., $t_{0-0} \neq 0$, $t_{U-U} \neq 0$, and $t_{0-U} \neq 0$. Here we have in mind this second nontrivial possibility, which results for large enough U in a density of states which consists of three bands: a 'metallic' band due to free sites, a lower Hubbard band (LHB), and an upper Hubbard band (UHB). The Hubbard bands result from the electronic states of correlated atoms above the metal–insulator transition. Of course, the Hubbard bands change their spectral weights in the usual way [26], and we do not discuss here the filling dependence.

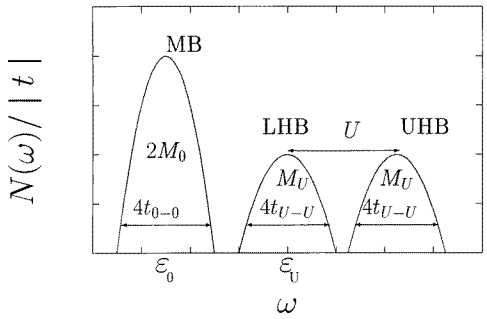

Figure 5. A schematic diagram of the density of states $N(\omega)$ for the model of superlattice (1)—the 'three bands' (MB—metallic, LHB/UHB—lower/upper Hubbard) represent $N(\omega)$ in the 'toy model' for $\varepsilon_0 = 0$ and typical parameters. For convenience, the total number of available states in each band ($2M_0$ and M_U, respectively) refers to the model with half-filled correlated orbitals.

The electrons filling the system may be then allocated to one of the three bands: if they occupy free sites—to the 'metallic' band (MB), and if they occupy the correlated atoms—either to the LHB, or to the UHB. This simplified model of the density of states $N(\omega)$ is shown in figure 5. The MB may accommodate $2M_0$ electrons, where M_0 is the total number of free sites. The corresponding capacities of the LHB and UHB at half-filling of the correlated atoms are both M_U.

Taking $\varepsilon_U = 0$, let us consider the changes of the electron distribution as the parameter ε_0 is varied. For $\varepsilon_0 < 2(t_{0-0} + t_{U-U})$ (note that both $t_{0-0} < 0$ and $t_{U-U} < 0$), all electrons will fall into the MB band, provided that $N < 2M_0$. Only when $N > 2M_0$ will the MB become full, with all of the free sites doubly occupied, and will the electrons start to occupy first the LHB, and, if $N > 2M_0 + M_U$, also the UHB, with the average density at any repulsive site $\langle n_{U,\sigma} \rangle = 0.5(N - 2M_0)/M_U$. For $\varepsilon_0 > 2t_{0-0} + 2t_{U-U}$, the MB starts to overlap with the LHB (and if we relax the assumption about noninteracting sublattices, there will be not only an overlap but also a substantial hybridization between the bands). If $\varepsilon_U < \varepsilon_0 < U$, the MB falls in between the LHB and the UHB. For the present parameters of the model, one expects the strongest overlap (one effective band) when $\varepsilon_0 = U/2$, provided that U is not too large.

4.2. Half-filled superlattices

In order to substantiate the qualitative picture of section 4.1, we determined the spectral densities of the superlattices considered, and studied their changes as a function of ε_0. We

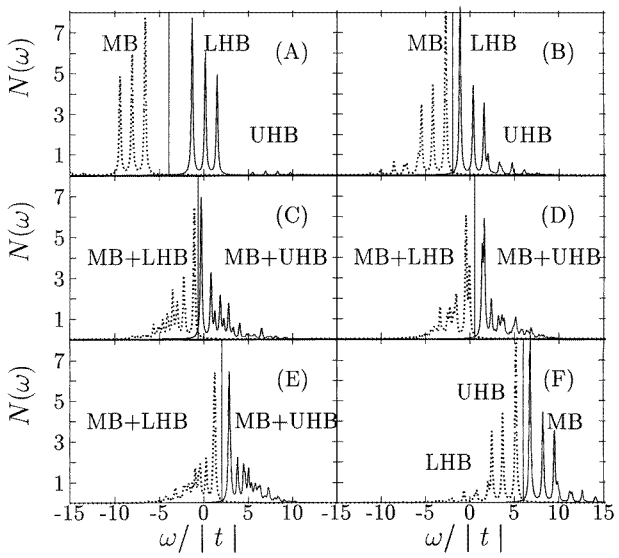

Figure 6. The one-particle spectral density $N(\omega)$ for the half-filled $M = 6$ cluster, $L_0 = L_U = 3$, with PBC at $U = 4|t|$. Dotted and solid lines correspond to PES, $N_{\mathrm{PES}}(\omega)$, and to IPES, $N_{\mathrm{IPES}}(\omega)$. Panels (A) to (F) correspond to different values of $\varepsilon_0 = -8$, -4, -2, 0, 4, and 8, in units of $|t|$. Note that the three bands, MB, LHB and UHB, are separated in panels (A), (B), and (F), while in the intermediate regime where $0 \leqslant \varepsilon_0 \leqslant 4|t|$, these bands hybridize. The vertical line shows the Fermi level.

define the one-particle spectral densities for photoemission (PES) [18, 27]:

$$N_{\mathrm{PES}}(\omega) = \sum_{in\sigma} |\langle \psi_n^{N-1} | c_{i\sigma} | \psi_0^N \rangle|^2 \delta(\omega + E_n^{N-1} - E_0^N) \tag{11}$$

and for inverse photoemission (IPES):

$$N_{\mathrm{IPES}}(\omega) = \sum_{in\sigma} |\langle \psi_n^{N+1} | c_{i\sigma}^\dagger | \psi_0^N \rangle|^2 \delta(\omega - E_n^{N+1} + E_0^N). \tag{12}$$

These expressions can be computed directly by determining the ground state of an N-electron system, $|\psi_0^N\rangle$, and the excited states of $N+1$ and $N-1$ systems, $|\psi_n^{N\pm1}\rangle$, respectively [15, 16]. We have studied the simplest case represented by the $M = 6$ cluster, with $L_0 = 3$ and $L_U = 3$, using PBC. The results obtained at half-filling are shown in figure 6. (The reference zero energy corresponds to the ground-state energy of the half-filled $M = 6$ cluster.)

One finds gradual modifications of the total spectral density, $N(\omega) = N_{\mathrm{PES}}(\omega) + N_{\mathrm{IPES}}(\omega)$, in agreement with the qualitative predictions of the toy model. At large negative $\varepsilon_0 = -8|t|$ (figure 6(A)) one finds the structures located at around $\omega = 0$, with the width of approximately $4|t_{0-0}|$. The lower (PES) part corresponds to the MB, while the upper (IPES) part corresponds to the LHB of the correlated atoms. The peaks found in the spectra are influenced by finite-size effects. Their number agrees with the allowed number of occupied one-particle states. Due to covalency within the superlattice, the correlated orbitals are partly occupied. However, the interference effects in the wave function make the weight of the UHB still very small [6]. Both the LHB and the UHB have approximately the width $4t_{U-U}$. In fact, to a good approximation, the electronic structure in this case consists of the bonding occupied states of the MB, and the unoccupied antibonding states of the LHB,

with a gap of about $\varepsilon_{gap} = 5.34$. Therefore, the system is an insulator. We note that the spectrum is almost symmetric with respect to $\omega = -4|t|$, which is a consequence of the particle–hole symmetry of the Hamiltonian at $U = 0$.

Increasing ε_0 results in a gradual closing of the gap, and in increasing weight of the UHB. The case where $\varepsilon_0 = -4|t|$ (figure 6(B)) still has a small gap of $1.7|t|$; and the MB and the LHB almost overlap. When the Drude peaks are calculated and a proper extrapolation from data (using at least two different cluster sizes) is made, we find that the system is still a weak insulator. This insulating behaviour vanishes at $\varepsilon_0 \simeq -2|t|$, and the MB and the LHB overlap, as shown in figure 6(C). Further increase of ε_0 results in even stronger hybridization between different subbands, and in the increasing occupancy of the UHB, i.e. in increasing double occupancies of the repulsive sites (figure 6(D)). This in turn increases the tendency of the system towards antiferromagnetism, and this tendency is independent of the superlattice structure, i.e., occurs for different L_0 and L_U, as discussed in section 5.1. The strongest AF correlations occur in the present case at $\varepsilon_0 = 2|t|$ (figure 6(E)). Further increase of ε_0 results in a gradual suppression of AF correlations, as the correlated orbitals are more than half-filled. Hybridization between the atoms of different kinds is weaker, and the metallic band moves above the UHB, as shown for $\varepsilon_0 = 8|t|$ in figure 6(F). The structure around $12|t|$ corresponds to a higher-order satellite which originates from the UHB. However, most of the weight in the UHB belongs to the PES spectrum, which indicates that the correlated orbitals are almost completely filled.

5. Magnetic properties

5.1. Correlation functions

The magnetic properties of 1D superlattices were discussed by Paiva and Santos [5], and we address here a few aspects not covered by this analysis, namely the dependences of the magnetic correlations on the energy splitting between the one-particle energies of two atoms, Δ, and on the value of Coulomb interaction U. Thereby, we consider different systems at and away from half-filling.

The magnetic correlation function in a paramagnetic system is defined as follows [5]:

$$\langle \boldsymbol{S}_i \cdot \boldsymbol{S}_j \rangle = \frac{3}{4} \langle m_i m_j \rangle \tag{13}$$

where $m_i = n_{i\uparrow} - n_{i\downarrow}$ corresponds to zth component of the spin at site i, and $i, j = 1, 2, \ldots, M$. Note that for $i = j$ it defines local moments [28, 29]:

$$\langle \boldsymbol{S}_i^2 \rangle = \frac{3}{4}(n - 2\langle n_{i,\downarrow} n_{i,\uparrow} \rangle). \tag{14}$$

The latter function is a measure of the localization, as for a half-filled metal ($n = 1$) one finds that $\langle \boldsymbol{S}_i^2 \rangle = 3/8$, while for localized electrons at half-filling one has $\langle n_{i\downarrow} n_{i\uparrow} \rangle = 0$, and $\langle \boldsymbol{S}_i^2 \rangle = 3/4$. The intersite correlation functions allow one to investigate the antiferromagnetic (AF) correlations, and their dependence on the structure of the cluster.

It is convenient to introduce average electron densities per free and correlated atom:

$$\begin{aligned} \overline{\langle n_{0\sigma} \rangle} &= \frac{1}{M_0} \sum_{i \in F}^{M_0} \langle n_{i\sigma} \rangle \\ \overline{\langle n_{U\sigma} \rangle} &= \frac{1}{M_U} \sum_{i \in R}^{M_U} \langle n_{i\sigma} \rangle \end{aligned} \tag{15}$$

and local moments per free and correlated atom, defined as follows:

$$\overline{\langle \boldsymbol{S}_0^2 \rangle} = \frac{1}{M_0} \sum_{i \in F}^{M_0} \langle \boldsymbol{S}_i^2 \rangle$$
$$\overline{\langle \boldsymbol{S}_U^2 \rangle} = \frac{1}{M_U} \sum_{i \in R}^{M_U} \langle \boldsymbol{S}_i^2 \rangle \tag{16}$$

where M_0 and M_U are the total numbers of free and repulsive atoms within the cluster, respectively.

As expected, the occupation of the free sites decreases with increasing ε_0, and the electrons are transferred to the repulsive sites. If $\langle n_{0\sigma} \rangle$ reaches the value 0.5, then the local magnetic moments on the free-site sublattice will be maximal; if $\langle n_{U\sigma} \rangle = 0.5$, the same holds for the repulsive sites of the sublattice considered. On the other hand, if the MB is completely filled, we expect zero magnetic effect on the free sites. Schematic diagrams showing the qualitative predictions of the toy model are shown in figure 7.

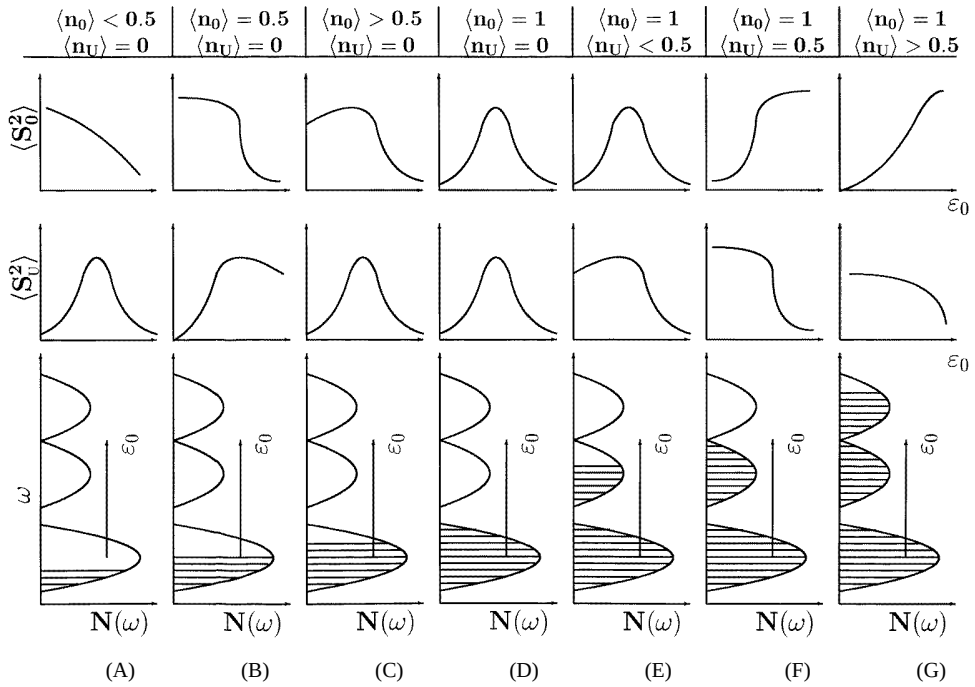

Figure 7. A schematic diagram of the dependence of the local moments, $\overline{\langle S_0^2 \rangle}$ and $\overline{\langle S_U^2 \rangle}$, on a free/repulsive site as functions of ε_0. Different cases are organized in separate columns corresponding to the total number of electrons increasing to the right. With increasing ε_0 the electrons move from free to correlated orbitals, causing the changes of local moments.

5.2. Local moments at half-filling

Let us start the analysis of magnetic properties with the half-filled systems. As expected, the occupation of the free sites decreases with increasing ε_0, and the electrons are transferred to the repulsive sites. If $\langle n_{0\sigma} \rangle$ reaches the value 0.5, the local magnetic moments on the free

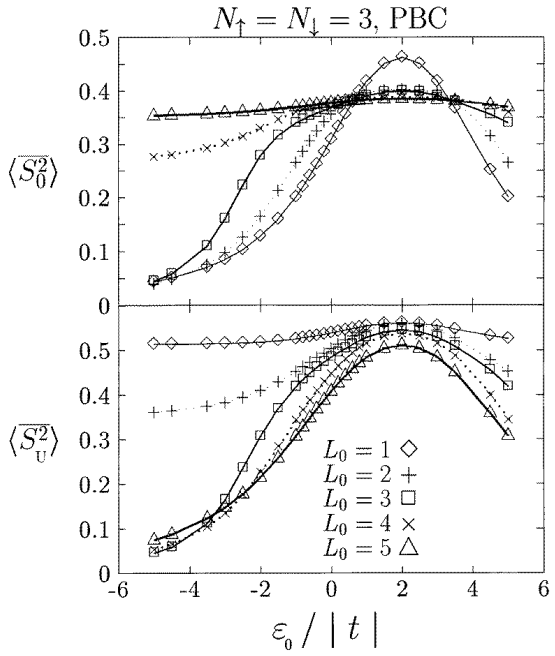

Figure 8. The average local moments, $\langle \overline{S_0^2} \rangle$ and $\langle \overline{S_U^2} \rangle$, at free and repulsive sites, respectively, for different values of ε_0, as obtained for the $M = 6$ cluster with ABC at half-filling ($n = 1$) and $U = 4|t|$, with different total numbers of free sites L_0.

sites are maximal; if $\langle n_{U\sigma} \rangle = 0.5$, the same holds for the repulsive sites of the sublattice considered. On course, if ε_0 is much lower than ε_U, the MB is almost completely filled, and the LHB is almost completely empty, as shown in figure 7, and one expects no magnetic effects. Indeed, in such a case the magnetic moment of the free layers is close to zero, but the local moments at the repulsive sites have already formed at around $\varepsilon_0 = -4|t|$, if there are only a few free atoms ($L_0 = 1$ and 2 in figure 8). With increasing ε_0, the local moments form at the correlated sites also, for superlattices with lower densities of correlated sites ($L_0 = 3$, 4, and 5). In fact, the local moments $\langle \boldsymbol{S}_U^2 \rangle$ are maximal at around $\varepsilon_0 = 2|t|$, which corresponds to the particle–hole-symmetric spectrum at the value considered, $U = 4|t|$.

It is interesting that the local moments at correlated atoms are almost independent of the type of the superlattice, which confirms that the local moments form solely due to on-site Coulomb interaction U. The moments $\langle \boldsymbol{S}_U^2 \rangle \simeq 0.5$ were found at $\varepsilon_0 = 2|t|$ and $U = 4|t|$, which is well above the band limit, and indicates gradual localization of electrons in the correlated orbitals. In contrast, the moments in uncorrelated orbitals, $\langle \boldsymbol{S}_0^2 \rangle \simeq 3/8$, remain close to the independent-electron limit, if the uncorrelated atoms form clusters of at least two atoms. However, a single uncorrelated atom is strongly polarized, and we find $\langle \boldsymbol{S}_0^2 \rangle \simeq 0.46$ at $\varepsilon_0 = 2|t|$ and $U = 4|t|$, as shown in figure 8 for $L_0 = 5$.

The interchange of the local magnetic moment between free and repulsive sites was reported previously in reference [5] for systems below half-filling. Here a similar effect was detected for a half-filled system, and it is found that it follows from the change of L_0 and L_U, or more precisely from changing their ratio.

The local moments at half-filling increase quite quickly in the correlated orbitals with increasing value of U, as shown in figure 9. The data for $\langle \boldsymbol{S}_U^2 \rangle$ show that the moment

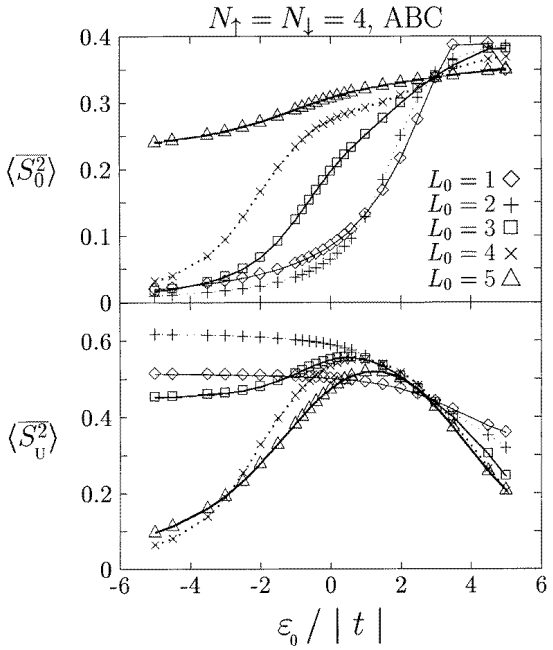

Figure 9. The local moments on the uncorrelated (top) and correlated (bottom) orbitals ($\langle \overline{S_0^2} \rangle$ and $\langle \overline{S_U^2} \rangle$, respectively) for increasing local interactions $U/|t|$, as obtained for the $M = 6$ clusters at half-filling ($n = 1$) with different L_0/L_U textures, and for $\varepsilon_0 = U/2$.

formation is robust and does not depend on the local structure of the superlattice—the moments are very close to each other for a given value of U, regardless of the type of the superlattice, and only a rather weak enhancement is found due to clustering of correlated atoms, represented by the cluster with $L_U = L_0 = 3$.

There are more differences in the behaviour of the free orbitals. Although in principle no local moments are expected, one may suspect that the moments could be induced by the correlations between the correlated and uncorrelated orbitals. Such correlations are weak as long as the free orbitals form islands in between the correlated ones (e.g., the clusters with $L_0 = 2$, $L_U = 1$, and $L_0 = L_U = 3$), but are enhanced for single atoms with uncorrelated orbitals (see $\langle S_0^2 \rangle$ for the cluster with $L_0 = 1$, $L_U = 2$ in figure 9).

5.3. Local moments away from half-filling

Up to now, to focus our attention, we have analysed half-filled systems using an $M = 6$ cluster with different values of L_0 and L_U. Sticking to the same systems, we now consider different fillings: $n = 8/6$ and $n = 4/6$. The results of numerical calculations are displayed in figures 10 and 11.

For filling larger than $n = 1$, we expect the MB to be completely filled at low energy ε_0, and thus that the system is an insulator, whereas the UHB has unoccupied states. Therefore, one expects the local magnetic moments to behave like those shown qualitatively in the last few columns of figure 7. As the ε_0-parameter increases, the system undergoes an insulator–metal transition (the $L_0 = 1$, 2, and 3 curves in figure 10). This is consistent with the values of D determined, as reported in section 3.2. However, the point of the transition itself shifts

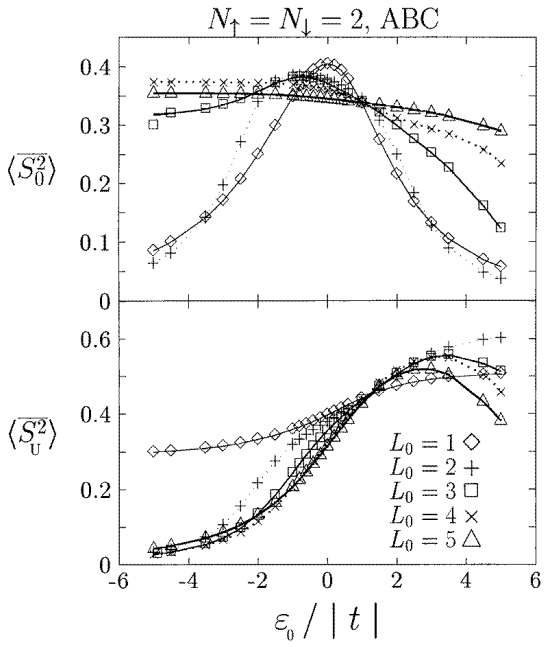

Figure 10. As figure 8, but above half-filling with $n = 1.33$.

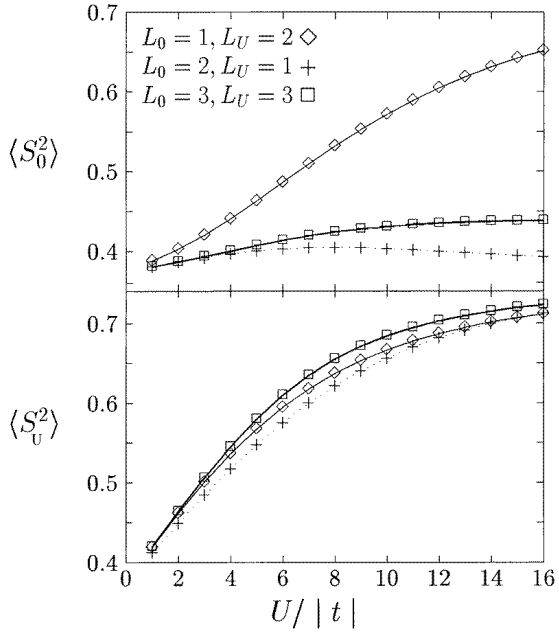

Figure 11. As figure 8, but below half-filling with $n = 0.67$.

in accord with the changes of the filling. In contrast, no metal–insulator transition was found at $L_0 = 4$ and 5, and the systems are metallic.

The local moments found in figure 10 agree reasonably well with the expected qualitative dependence. The local moments $\langle \boldsymbol{S}_U^2 \rangle$ are more pronounced at lower values of ε_0 than at $n = 1$, and at $L_0 = 2$ one finds even large local moments $\langle \boldsymbol{S}_U^2 \rangle \simeq 0.62$ down to $\varepsilon_0 = -4|t|$. This follows from the particular filling which matches single occupancy of the correlated

sites ($L_U = 4$), and the remaining electrons give double occupancies at free sites ($L_0 = 2$). In contrast to the half-filled case, there are no induced moments at free atoms in this case, and only a weak enhancement of $\langle \boldsymbol{S}_0^2 \rangle$ could be detected at $L_0 = 1$.

For an electron filling smaller than half-filling, one starts from the opposite situation at large negative ε_0: the MB is not completely filled and the LHB is empty. Thus, one finds at first no local moments on free atoms, if their density is small ($L_0 = 1$ and 2 in figure 11), but if $2M_0 > N_\uparrow + N_\downarrow$, one finds values of $\langle \boldsymbol{S}_0^2 \rangle$ close to the band limit (see $L_0 = 3$, 4, and 5 in figure 11). The system behaves like a metal, at least for the range $-U < \varepsilon_0 < U$, and we have verified that $D \neq 0$ in this case.

We note that the case of low density of free atoms is again resulting in enhanced local moments, but now for $\varepsilon_0 > \varepsilon_U + U$. As expected, the values of $\langle \boldsymbol{S}_U^2 \rangle$ for a given value of ε_0 at $n = 0.67$ are identical with the respective values obtained with $-\varepsilon_0 + U$, and large local moments $\langle \boldsymbol{S}_U^2 \rangle \simeq 0.62$ are found at $\varepsilon_0 \simeq 4|t|$ (not shown). The same particle–hole symmetry arises for the data for $\langle \boldsymbol{S}_0^2 \rangle$, and we find a Gaussian shape for $L_0 = 1$ and 2 which corresponds to the changing number of electrons and holes for $n = 1.33$ and $n = 0.67$ within the free orbitals, respectively.

If the electron levels are degenerate, the local moments are close to the limit of independent electrons for low electron density; an example with $L_0 = L_U = 2$ with $M = 8$ is detailed in table 1, where $\langle \boldsymbol{S}_U^2 \rangle \simeq \langle \boldsymbol{S}_0^2 \rangle$ for $n \leqslant 0.75$. Intermediate values of U only lead to the formation of moderate local moments in the correlated orbitals at $n = 1$ ($\langle \boldsymbol{S}_U^2 \rangle = 0.47$).

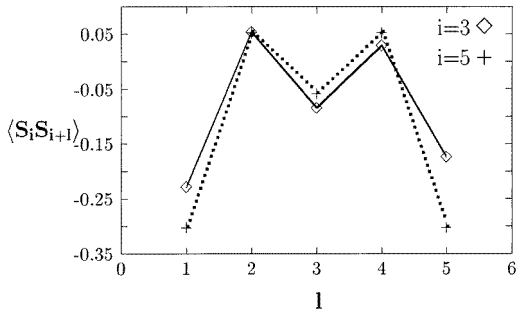

Figure 12. The intersite spin–spin correlations $\langle \boldsymbol{S}_i \cdot \boldsymbol{S}_{i+l} \rangle$ as functions of the distance from the reference site $i = 3$ and 5, as obtained for the $M = 6$, $L_0 = L_U = 3$ cluster at half-filling, using PBC ($\varepsilon_0 = 0$, $U = 4|t|$). The alternating values indicate the tendency of the system towards spin-density waves (SDW).

5.4. Intersite spin correlations

The systems at half-filling exhibit AF correlations, indicating their proximity to the spin-density-wave instability. This behaviour is quite remarkable, as the AF correlations include also the uncorrelated atoms, as shown in figure 12. We have verified that the AF correlations exist for different clusters modelling superlattices. Here we present only the most unfavourable case of $L_0 = L_U = 3$ for a cluster of $M = 6$ sites. At the intermediate value $U = 4|t|$ one finds that $\langle \boldsymbol{S}_i \cdot \boldsymbol{S}_{i+1} \rangle = -0.26 \pm 0.04$, taking the reference value as either $i = 3$ or $i = 5$; for the other values of i the results are similar. In the first case one starts from a free atom and a neighbour is correlated, while in the second case the two atoms involved are correlated. The symmetry of the cluster imposes the symmetric shape

of $\langle \boldsymbol{S}_i \cdot \boldsymbol{S}_{i+l} \rangle$ with respect to $l = 3$ for $i = 5$, and $\langle \boldsymbol{S}_i \cdot \boldsymbol{S}_{i+5} \rangle = \langle \boldsymbol{S}_i \cdot \boldsymbol{S}_{i+1} \rangle = -0.30$. The spin–spin correlation function of two uncorrelated atoms is considerably lower; e.g., $\langle \boldsymbol{S}_i \cdot \boldsymbol{S}_{i+5} \rangle = -0.18$ is found for $i = 3$.

Altogether, the spin–spin correlations are found to be primarily of short-range character. As shown in figure 12, the signs of $\langle \boldsymbol{S}_i \cdot \boldsymbol{S}_{i+l} \rangle$ alternate, and one finds for degenerate one-particle levels $\varepsilon_0 = \varepsilon_U = 0$ at $U = 4|t|$ that $|\langle \boldsymbol{S}_i \boldsymbol{S}_{i+l} \rangle| < 0.10$ if $1 < l < M - 1$.

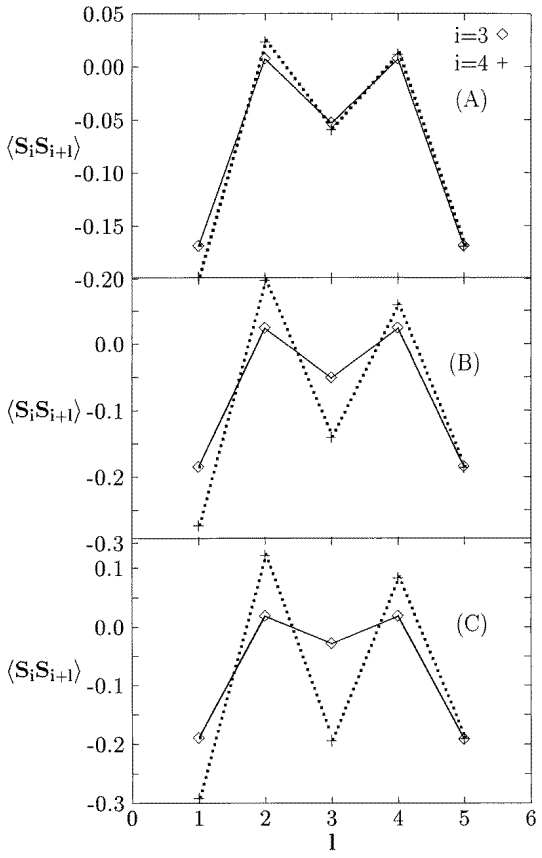

Figure 13. The intersite spin–spin correlations $\langle \boldsymbol{S}_i \cdot \boldsymbol{S}_{i+l} \rangle$ as functions of the distance from the reference site $i = 3$ and 4, as obtained for the $M = 6$, $L_0 = L_U = 3$ cluster at half-filling using PBC and particle–hole-symmetric structure ($\varepsilon_0 = U/2$), for different values of U: (A) $U = 2|t|$, (B) $U = 8|t|$, and (C) $U = 16|t|$. The alternating values indicate the tendency of the system towards SDW. The AF correlations and the frustration of the magnetic interactions increase with increasing U.

We investigated also the changes of AF spin–spin correlations with increasing values of U. An example for the particle–hole-symmetric model with $\varepsilon_0 = U/2$ shown in figure 13 demonstrates that these correlations develop quite quickly, and are already quite significant at $U = 2|t|$. Thus, the SDW-like state forms at small U, and the amplitude of the spin–spin correlations steadily increases with increasing U. The case of $U = 8|t|$ already represents relatively strong localization of electrons (see figure 9), and the spin–spin correlations are almost in changed on increasing U from $8|t|$ to $16|t|$.

6. Discussion and summary

We have shown that the electronic structure and the magnetic properties of superlattices may be well understood starting from the effective model which originates from the atomic limit, and consists of three subbands, a MB for the free atoms, and two Hubbard subbands: the LHB and UHB for the correlated atoms. The superlattice is characterized by a competition between localization of electrons on the correlated orbitals, and the accompanying formation of local moments, and the hybridization between the free and correlated orbitals which results in the metallic behaviour. By varying the splitting between the one-particle levels for free and correlated orbitals, $\Delta = \varepsilon_0 - \varepsilon_U$, one realizes a transition from an insulating to a metallic regime. The latter may in principle be considered as an effective hybridized broad band, provided that the Coulomb interaction U is not too large (in units of $|t|$).

The model considered has a particle–hole-symmetric spectrum at $\varepsilon_U = 0$, and $\varepsilon_0 = U/2$, where the hybridization and the metallic behaviour are strongest at half-filling; otherwise the particle–hole symmetry is explicitly broken. However, varying the total filling n and taking $\varepsilon_0 \leqslant U/2$, one has already covered all of the physically different cases, as for $\varepsilon_0 \geqslant U/2$ the electronic properties are equivalent in terms of hole density, $n_h = 2 - n$. Thus, we limited ourselves in most cases to discussing the cases where $\varepsilon_0 \leqslant U/2$. Below, we discuss the characteristic behaviour found depending on the value of Δ, and electron filling n.

Most of the characteristic features can be detected using large negative $\varepsilon_0 \ll -|t|$, and $\langle n_{0\sigma}\rangle \simeq 1$, $\langle n_{U\sigma}\rangle \simeq 0.5$. In this case the moments at the repulsive sites are well formed and dominate the magnetic behaviour; only the repulsive sites are magnetic, but they are separated by the nonmagnetic (doubly occupied) free sites. Thus, the system is not conducting. The clusters considered do not allow us to reach conclusions regarding the magnetic ordering of the local moments in this regime, but it is expected that possible long-range order in the thermodynamic limit will strongly depend on the sequence of correlated and uncorrelated orbitals, given by L_U and L_0.

If $\varepsilon_0 \ll -|t|$, and the total electron density is decreased to $\langle n_{0\sigma}\rangle \simeq 1$, $\langle n_{U\sigma}\rangle < 0.5$, the MB hybridizes more strongly with the partially filled LHB of the correlated orbitals, and the system is a weak conductor, with an increasing conductivity for increasing ε_0 and approaching $\varepsilon_0 \simeq \varepsilon_U$ (figure 6(C)). The typical local moment results are shown in figure 10 ($L_0 = 3$, 4, and $n = 8/6$), and in figure 8 ($L_0 = 1$, 2, 3, and $n = 1$). For negative ε_0, electrons doubly occupy the free sites; for positive ε_0, local pairs at free orbitals are broken and one finds the density distribution close to one electron per (free or correlated) site. This leads to AF short-range correlations, and possibly also to the AF long-range order, if the magnetic interactions are not frustrated. While the latter could not be investigated in our finite clusters, the short-range AF correlations are found to be generic, and to depend only weakly on the specific type of superlattice (i.e., on L_0 and L_U).

Further decrease of the total electron density results for large negative ε_0 in a partially filled MB, and an empty LHB of the correlated sites (figures 6(A) and 6(B)). Now the repulsive layers form a barrier to the conduction (in real space), and only when ε_0 is increased, and the MB and LHB start to hybridize more strongly, may the system become conducting (see table 3, for $n = 0.5$). The almost empty correlated orbitals give a negligible contribution to the magnetism, and the magnetic correlations due to free sites dominate (cf. figure 11 for $L_0 = 3$ and $n = 4/6$ together with figure 8 and figure 10).

We presented the results obtained in most cases for small clusters of $M = 6$ sites. The conclusions, however, concern the local properties of the systems, and thus are representative for larger clusters as well. To confirm this, we considered almost all of the possible systems with different M but fixed density n (note that N must be an integer). The typical examples

are: (i) $M = 4$ and $M = 8$ for $L_0 = L_U = 2$, with the fillings $n = 2/4$ and $n = 6/4$; (ii) $M = 5$ and $M = 10$ for $L_0 = 1$, $L_U = 4$, with the fillings $n = 4/5$ and $n = 6/5$. The qualitative results agreed with expectations, and in particular the weights of the Drude peak showed very systematic behaviour (summarized in table 3). These results lead us to believe that the small-cluster results discussed are also representative for the properties of infinite lattices.

Summarizing, we studied the Hubbard-type Hamiltonian defined for 1D superlattices. Using the Lanczos algorithm, we computed (exactly) ground-state properties, local magnetic moments, the Drude peak amplitudes, and the spectral functions for small clusters. While the results obtained confirm the earlier results of Paiva and Santos [5] for magnetic properties such as local magnetic moments, frustration of magnetic interactions, and magnetic surface–bulk effects, they could be extended by studying the conductivity of the systems, and the dependence of the Drude peak on the position of the one-particle level ε_0, and on the lattice filling n. Varying these quantities, one obtains both metallic and insulating phases, which has important implications for the magnetic properties. We would like to emphasize that the qualitative features could always be predicted using a simple model of the electronic structure which consists of three bands. It can therefore be considered as a useful tool which allows one to avoid time-consuming numerical diagonalization. Altogether, one finds that the magnetic and electronic properties of superlattices are more complex than those of homogeneous systems, and we believe that the changes detected in the conductivity could be of importance for real systems, where the carrier density n and the level splitting Δ might be changed by doping and by external parameters.

We believe that the situation given by $U/|t| \simeq 4$ studied primarily in the present contribution is representative for superlattices with 3d transition metal magnetic layers within nonmagnetic media. However, one has to realize that the nondegenerate model for d orbitals may serve only as a qualitative model describing the localization of electrons and the formation of local moments due to Coulomb interaction. A more quantitative description would require extending the model to degenerate d orbitals at the correlated sites [30]. The Hund's rule exchange would then help to form the local moments, and it is expected that the magnetic correlations would be enhanced.

Acknowledgment

We acknowledge partial support by the Polish Committee of Scientific Research (KBN), Project No 2 P03B 144 08.

References

[1] Baibich M N, Broto J M, Fert A, Nguyen Van Dau F, Petroff F, Eitenne P, Creuzet G, Friederich A and Chazelas J 1988 *Phys. Rev. Lett.* **61** 2472
[2] Parkin S S P, More N and Roche K P 1990 *Phys. Rev. Lett.* **64** 2304
[3] Grünberg P, Demokritov S, Fuss A, Vohl M and Wolf J A 1991 *J. Appl. Phys.* **69** 4789
[4] Koorevaar P, Kes P H, Koshlev A E and Aarts J 1994 *Phys. Rev. Lett.* **72** 3250
[5] Paiva T and Santos R R 1996 *Phys. Rev. Lett.* **76** 1126
[6] Eskes H, Oleś A M, Meinders M and Stephan W 1994 *Phys. Rev.* B **50** 17 980
[7] Hubbard J 1963 *Proc. R. Soc.* A **276** 238
[8] Jullien R and Martin R M 1982 *Phys. Rev.* B **26** 6173
[9] Rościszewski K and Oleś B 1993 *J. Phys.: Condens. Matter* **5** 7289
[10] Fourcade B and Sproken G 1984 *Phys. Rev.* B **29** 5096
[11] Nishino T 1992 *J. Phys. Soc. Japan* **61** 3651
[12] Lanczos C 1950 *J. Res. NBS* **45** 255

[13] Heine V 1980 *Solid State Physics* vol 35 (New York: Academic) p 1
[14] Ralston A 1985 *A First Course in Numerical Analysis* (New York: McGraw-Hill)
[15] Gagliano E R and Balseiro C A 1987 *Phys. Rev.* B **38** 11 766
[16] Gagliano E R and Balseiro C A 1987 *Phys. Rev.* B **59** 2999
[17] Lin H Q and Gubernatis J E 1993 *Comput. Phys.* **7** 400
[18] Fulde P 1991 *Electron Correlation in Molecules and Solids (Springer Series in Solid-State Sciences 100)* ed C Cardona, P Fulde, K von Klitzing and H J Queisser (Berlin: Springer)
[19] Shastry B S and Sutherland B 1990 *Phys. Rev. Lett.* **65** 243
[20] Shastry B S 1992 *Mod. Phys. Lett.* B **6** 1427
[21] Scalapino D J, White S R and Zhang F C 1992 *Phys. Rev. Lett.* **68** 2830
[22] Scalapino D J, White S R and Zhang F C 1993 *Phys. Rev.* B **47** 7995
[23] Wagner J, Hanke W and Scalapino D J 1991 *Phys. Rev.* B **43** 10 517
[24] Fye M R, Mastins M J and Scalapino D J 1991 *Phys. Rev.* B **44** 6909
[25] Maldague F P 1977 *Phys. Rev.* B **16** 2437
[26] Meinders M, Eskes H and Sawatzky G A 1993 *Phys. Rev.* B **48** 3916
[27] Dagotto E D 1994 *Rev. Mod. Phys.* **64** 763
[28] Stollhoff G and Thalmeier P 1981 *Phys. Rev.* B **16** 2437
[29] Oleś A M 1982 *J. Phys. C: Solid State Phys.* **15** 2745
[30] Fleck M, Oleś A M and Hedin L 1997 *Phys. Rev.* B **56** 3159